The Vertical Structure of Annular Modes

ADITI SHESHADRI

Department of Earth System Science, Stanford University, Stanford, California

R. ALAN PLUMB AND ERIK A. LINDGREN

Department of Earth, Atmospheric, and Planetary Sciences, Massachusetts Institute of Technology, Cambridge, Massachusetts

DANIELA I. V. DOMEISEN

Institute for Atmospheric and Climate Science, ETH Zürich, Zurich, Switzerland

(Manuscript received 28 December 2017, in final form 21 May 2018)

ABSTRACT

Stratosphere–troposphere interactions are conventionally characterized using the first empirical orthogonal function (EOF) of fields such as zonal-mean zonal wind. Perpetual-winter integrations of an idealized model are used to contrast the vertical structures of EOFs with those of principal oscillation patterns (POPs; the modes of a linearized system governing the evolution of zonal flow anomalies). POP structures are shown to be insensitive to pressure weighting of the time series of interest, a factor that is particularly important for a deep system such as the stratosphere and troposphere. In contrast, EOFs change from being dominated by tropospheric variability with pressure weighting to being dominated by stratospheric variability without it. The analysis reveals separate tropospheric and stratospheric modes in model integrations that are set up to resemble midwinter variability of the troposphere and stratosphere in both hemispheres. Movies illustrating the time evolution of POP structures show the existence of a fast, propagating tropospheric mode in both integrations, and a pulsing stratospheric mode with a tropospheric extension in the Northern Hemisphere–like integration.

1. Introduction

The leading patterns of variability of the circulation of the extratropical troposphere and stratosphere are referred to as the ''annular modes'' (e.g., Thompson and Wallace 2000; Thompson et al. 2000) and are usually derived using empirical orthogonal function (EOF) analysis of meteorological fields such as geopotential height and zonal-mean zonal wind. In the troposphere, the first EOF of zonal-mean zonal wind has a dipolar structure straddling the eddy-driven jet, while the second EOF has a tripolar structure, with its primary extremum coincident with the latitude of the jet. Taken independently, the first EOF represents fluctuations in the latitudinal position of the jet, while the second EOF represents intensification and narrowing of the jet. However, under some circumstances, these two EOFs are not independent of each other (Sparrow et al. 2009) but are in fact manifestations of a single, coupled, underlying eigenmode of the underlying dynamical system governing the evolution in time of zonal-mean zonal wind anomalies (Sheshadri and Plumb 2017).

Extensive observational and modeling evidence suggests that fluctuations in the strength of the stratospheric polar vortex impact the tropospheric midlatitude jet and storm tracks (e.g., Baldwin and Dunkerton 2001). In turn, the variability of the extratropical winter stratosphere is influenced by the propagation and breaking of planetary-scale waves of tropospheric origin (e.g., Scaife and James 2000). Annular modes have been used to characterize these two-way interactions between the troposphere and stratosphere; for example, Baldwin and

Supplemental information related to this paper is available at the Journals Online website: https://doi.org/10.1175/JAS-D-17-0399.s1.

Corresponding author: Aditi Sheshadri, aditi_sheshadri@stanford.edu

DOI: 10.1175/JAS-D-17-0399.1

Dunkerton (1999, 2001) and others have noted a correlation between the first EOF in the stratosphere (representing changes in the strength of the polar vortex) and the tropospheric annular mode (representing latitudinal shifts of the midlatitude jet). Anomalous values of the annular mode in the stratosphere appear to be followed by like-signed anomalies in the troposphere, all the way to Earth's surface, and these anomalies can sometimes persist for longer than a month, a finding that has led to the suggestion that resolving stratospheric variability in a model could enhance seasonal forecasting (e.g., Baldwin et al. 2003; Tripathi et al. 2015; Scaife et al. 2016). Studies also suggest that the persistence of the midlatitude jet and storm tracks is larger in ''active'' periods in the lower stratosphere, that is, midwinter in the Arctic and spring in the Antarctic (Baldwin et al. 2003; Sheshadri and Plumb 2016; Byrne et al. 2017).

While the EOFs compactly and efficiently describe the fluctuations of the variable of interest and are frequently referred to as modes, they are not necessarily modes in the usual physical sense of being eigenmodes of the underlying dynamical system. Rather, the EOFs and their corresponding principal component (PC) time series depend on how the system is forced to produce the variability—and not just on the properties of the system modes themselves. Moreover, they are by construction orthogonal, whereas in general the system modes are not. Furthermore, the EOFs are dependent on how the data are weighted before performing the singular-value decomposition. The modes of the underlying linearized dynamical system describing the evolution in time of zonal-mean zonal winds can be revealed by principal oscillation pattern (POP) analysis (von Storch et al. 1988; Penland 1989). Sheshadri and Plumb (2017) showed that for tropospheric data only, the leading mode is complex, with a structure that involves at least two EOFs, and describes poleward propagation of zonal-mean zonal wind anomalies. The time scale associated with this mode is different from the decorrelation time of the leading EOF, indicating that in a fluctuation–dissipation framework, the time scale of relevance to climate model responses to external forcing may in some cases be very different from the annular-mode time scale. POP analysis has been applied to a range of problems in the climate system, such as the variability of the eastern Pacific (Penland and Sardeshmukh 1995), the Madden–Julian oscillation (von Storch and Xu 1990), and variations of sea level pressure in the low to middle latitudes of the Southern Hemisphere (Xu and von Storch 1990). Newman and Sardeshmukh 2008 used a linear inverse model to compare the effects of tropical diabatic heating and stratospheric variability on short-term extratropical tropospheric variability, treating the tropospheric and stratospheric streamfunctions (calculated at selected pressure levels) as separate.

In this paper we apply POP analysis to the coupled stratosphere–troposphere system, using idealized, perpetual-winter simulations. The model setup is described in section 2. Section 3 demonstrates that the modes that emerge from POP analysis are insensitive to pressure weighting of the zonal-mean zonal wind data. The space–time structure of the modes are described in section 4. A discussion of these results follows in section 5.

2. Model setup

The model is based on that of Polvani and Kushner (2002) and is identical to that of Sheshadri and Plumb (2017). The model is dry and hydrostatic, solving the global primitive equations with T42 resolution in the horizontal and 40 sigma levels in the vertical. Radiation and convection schemes are replaced by relaxation to a zonally symmetric equilibrium temperature profile identical to Held and Suarez (1994) in the troposphere. In the stratosphere (above 200 hPa), the equilibrium temperature profile is a perpetual-solstice version of the equilibrium temperature specifications used in Sheshadri et al. (2015) with winter conditions in the hemisphere of interest. As will be seen below, these choices result in a model configuration with reasonable annular-mode time scales in the Southern Hemisphere in the unforced case. Without any imposed source of planetary-scale waves (topography or diabatic heating) in the troposphere, the model produces a winter climatology that resembles that of the observed Antarctic stratosphere, with no stratospheric sudden warmings (SSWs). When planetary-scale waves in the model are forced with wave-2 diabatic heating in the troposphere [similar to the forcing used by Scott and Polvani (2006)], the frequency of SSWs increases with the amplitude of the forcing used. Here we present results from two model integrations: an unforced case and a strongly forced case with an SSW frequency of 0.48 events per 100 winter days, similar to that of the observed Arctic stratosphere (in which the SSW frequency is 6 decade^{-1} between the winters of 1957 and 2002; e.g., Charlton and Polvani 2007). The use of diabatic heating as a source of planetary-scale waves rather than topography enables one to compute EOFs all the way to the surface without having to deal with large portions of the midlatitudes being masked by topography. The form of diabatic heating used is

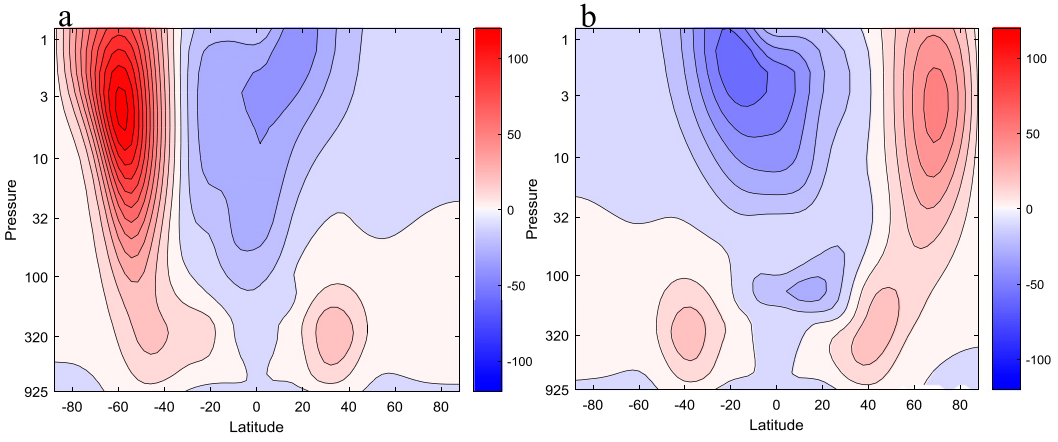

FIG. 1. Time-mean zonal-mean zonal winds for (a) the unforced and (b) the strongly forced integration. The contour interval is 10 m s^{-1}.

$$Q(\lambda,\varphi,p)=\begin{cases} q_0 \sin(2\lambda)\exp\left[-\frac{1}{2}\left(\frac{\varphi-\varphi_0}{\sigma_\varphi}\right)^2\right]\sin\pi\left[\frac{\log(p/p_0)}{\log(p_t/p_0)}\right], & p_t \le p \le p_0 \\ 0, & \text{otherwise} \end{cases}. \tag{1}$$

where λ is longitude, φ is latitude, p is pressure, $q_0 = 6\,\mathrm{K\,day^{-1}}$, $\varphi_0 = 45°\mathrm{N}$, $\sigma_\varphi = 0.175 \times 360/(2\pi)$, $p_0 = 800\,\mathrm{hPa}$, and $p_t = 200\,\mathrm{hPa}$. The integrations analyzed here are 13 000 days long, with the last 10 000 days used in the analysis. Figure 1 shows the winter climatology for the two integrations. Note that the core of the stratospheric jet is weaker and farther poleward in the forced case. The climatology and variability of integrations of this idealized model when planetary-scale waves are forced by diabatic heating are described in detail in Lindgren et al. (2018, manuscript submitted to *J. Geophys. Res. Atmos.*).

3. Independence of principal oscillation patterns under weighting

We follow the analysis of Sheshadri and Plumb (2017) in calculating and selecting the modes of interest. Some of their analysis is repeated here for clarity. Singular value decomposition of data poleward of 20° is used to calculate the EOFs (spatial patterns) and corresponding PCs:

$$\mathbf{X} = \mathbf{U}\boldsymbol{\Sigma}\mathbf{V}^{\mathrm{T}}, \tag{2}$$

where the variable used to perform (2) is $\sqrt{\cos\varphi}\,(\overline{u} - [\overline{u}])$, with or without a factor of $\sqrt{\delta p}$, where δp is the pressure thickness of the model level; u is zonal wind; φ is latitude; the square brackets represent the time average of daily data; and the overbar is the zonal average. The columns of $\mathbf{U}$ are the EOFs; the columns of $\mathbf{V}$ contain the normalized PCs, with $\boldsymbol{\Sigma}$ being the diagonal matrix containing the corresponding singular values σ. When the data are weighted by $\sqrt{\delta p}$, the EOFs are then de-weighted for presentation.

We consider a forced, linear, dynamical system of the form

$$\frac{\partial \mathbf{u}}{\partial t} + \mathbf{A}\mathbf{u} = \mathbf{f}. \tag{3}$$

An equation of this form has been used to describe fluctuations of zonal-mean wind about its climatological state, both with (e.g., Lorenz and Hartmann 2001, 2003; Chen and Plumb 2009; Byrne et al. 2016) and without (Ring and Plumb 2007, 2008; Lutsko et al. 2015; Hassanzadeh and Kuang 2016) vertical averaging. In the latter case, the validity of such a representation rests on a number of assumptions (Ring and Plumb 2008): that the mean flow is balanced, that variations of static stability are small, and that eddy feedback can be represented as a linear function of the instantaneous mean zonal wind anomaly. The latter assumption restricts the validity of (3) to time scales longer than those of baroclinic eddy life cycles.

The unforced system has modes described by the eigenvectors and eigenvalues of the operator $\mathbf{A}$; if these are known, then the response to any forcing $\mathbf{f}$ can be determined. However, in practice $\mathbf{A}$ is not known, primarily

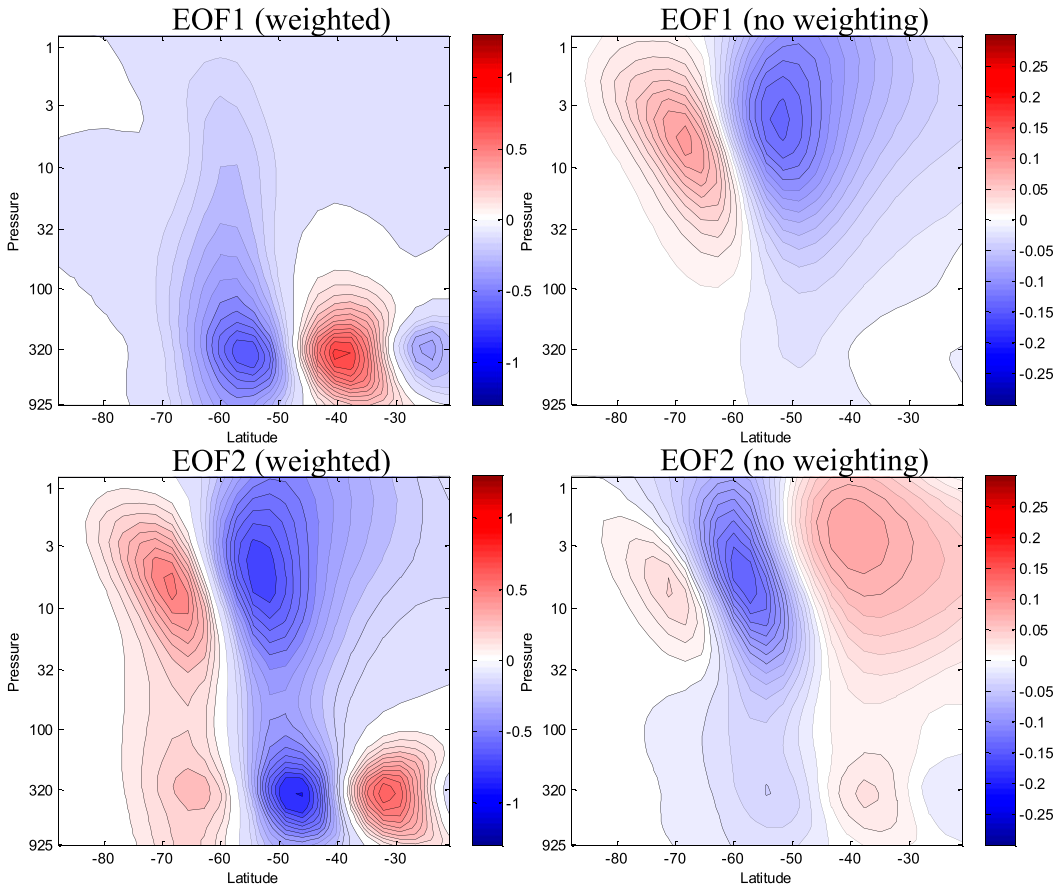

FIG. 2. The two leading EOFs of (left) pressure-weighted zonal-mean zonal wind and (right) zonal-mean zonal wind without any pressure weighting, from the unforced integration. The EOFs in the left panels explain (top) 37% and (bottom) 27% of variance and have decorrelation times of 19 and 13 days, respectively; while the EOFs in the right panels explain (top) 56% and (bottom) 12% of variance and have decorrelation times of 40 and 17 days, respectively.

because it includes the eddy feedback operator, a parameterization of which remains elusive. However, the modes are implicit in the observed behavior of the system, which can be used to determine the eigenvectors of $\mathbf{A}$ in the form of the principal oscillation patterns. Assuming that the observed fluctuations of u are the responses of a stable system described by (3) to white noise forcing, the eigenvectors of the matrix

$$\mathbf{G}(\tau) = \mathbf{C}(\tau)\mathbf{C}(0)^{-1}, \tag{4}$$

where

$$\mathbf{C}(\tau) = \mathbf{X}_{\tau}\mathbf{X}^{\mathrm{T}}. \tag{5}$$

is the lag covariance of the zonal wind anomalies (the subscript τ denotes evaluation at lag τ), are the eigenvectors of $\mathbf{A}$ (von Storch et al. 1988; Penland 1989). Thus, for a given lag τ, one can determine $\mathbf{G}(\tau)$and hence its eigenvectors. The primary difficulty, however, arises from the need to invert $\mathbf{C}(0)$, which can be problematic. The inverse is dominated by those components with the smallest singular values, that is, those that contribute least to the variance (Martynov and Nechepurenko 2004). For this reason, it has often been found expedient to improve the inversion by mapping the data onto a finite number of EOFs before applying (3) (e.g., Xu and von Storch 1990; Penland and Sardeshmukh 1995; Gritsun and Branstator 2007; Ring and Plumb 2008; Lutsko et al. 2015).

It is possible, however, to determine the POPs without the need to perform a matrix inversion by performing the calculations in EOF space, thereby diagonalizing the zero-lag covariance matrix (Penland 1989). Introducing the lag covariance of the normalized PCs

$$\hat{\mathbf{C}}(\tau) = \mathbf{V}_{\tau}^{\mathrm{T}}\mathbf{V}, \tag{6}$$

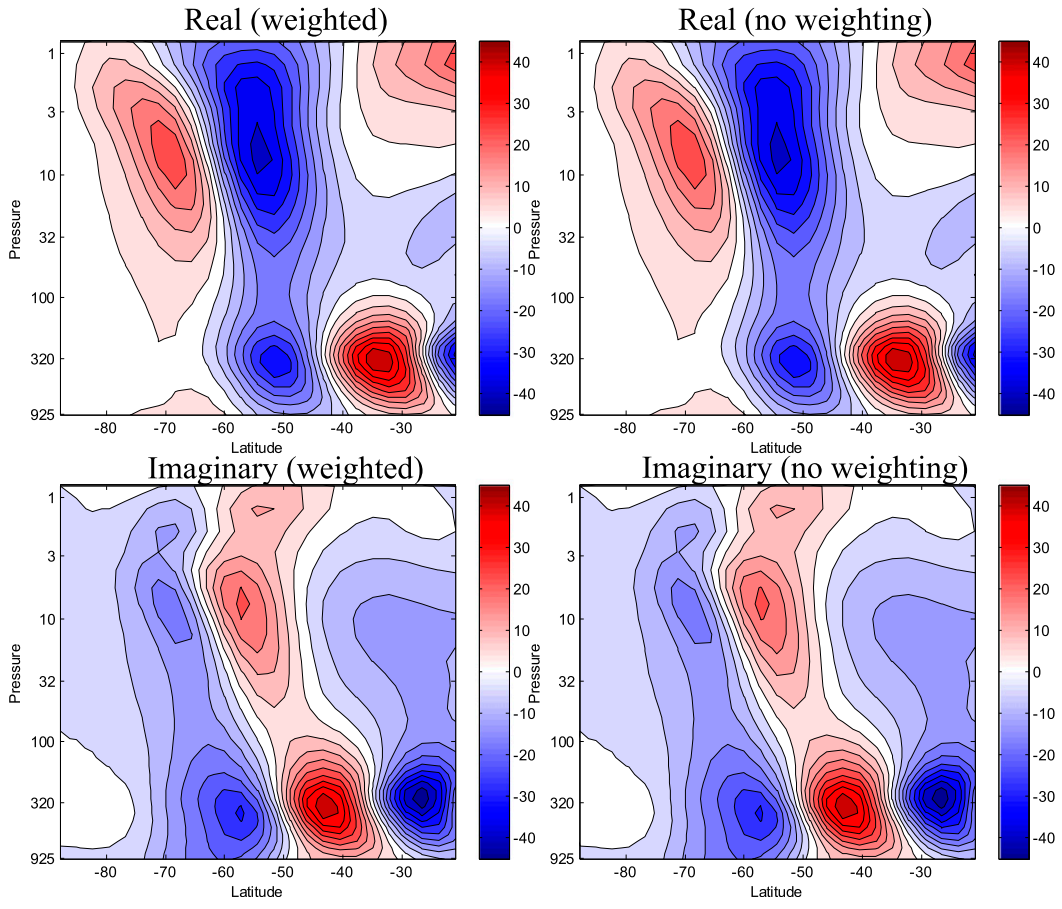

FIG. 3. (top) Real and (bottom) imaginary parts of the leading tropospheric POP computed from (left) EOFs of pressure-weighted zonal-mean zonal wind and (right) EOFs of zonal-mean zonal wind without any pressure weighting, from the unforced integration. Their corresponding eigenvalues are identical and correspond to a decay time of 39 days and a period of propagation of 126 days.

then (4), with (2), (5), and (6), gives

$$\mathbf{G}(\tau) = \mathbf{U\Sigma V}_\tau^{\mathrm{T}}\mathbf{V\Sigma U}^{\mathrm{T}}\mathbf{U\Sigma}^{-2}\mathbf{U}^{\mathrm{T}} = \mathbf{U\Sigma}\hat{\mathbf{C}}(\tau)\mathbf{\Sigma}^{-1}\mathbf{U}^{\mathrm{T}}.$$

Therefore, introducing the eigenvector decomposition of $\hat{\mathbf{C}}(\tau)$,

$$\hat{\mathbf{C}}(\tau) = \mathbf{W\Gamma}(\tau)\mathbf{W}^{-1}, \tag{7}$$

where $\mathbf{\Gamma}$ is the diagonal matrix of the eigenvalues, we have

$$\mathbf{G}(\tau) = \mathbf{U\Sigma W\Gamma}(\tau)\mathbf{W}^{-1}\mathbf{\Sigma}^{-1}\mathbf{U}^{\mathrm{T}} = \mathbf{Z\Gamma}(\tau)\mathbf{Z}^{-1}, \tag{8}$$

where the columns of the matrix

$$\mathbf{Z} = \mathbf{U\Sigma W} \tag{9}$$

are the POPs, the eigenvectors of $\mathbf{G}(\tau)$, and hence (von Storch et al. 1988; Penland 1989) the eigenvectors of the system matrix . The eigenvalues λ of $\mathbf{A}$ are not the same as those of $\mathbf{G}(\tau)$, but they are related through

$$\mathbf{\Gamma}(\tau) = \exp(-\mathbf{\Lambda}\tau), \tag{10}$$

where $\mathbf{\Lambda}$ is the diagonal matrix with elements λ. Hence,

$$\mathbf{A} = \mathbf{Z\Lambda Z}^{-1}. \tag{11}$$

Thus, taking this approach yields the POPs and their eigenvalues without the need to perform an explicit inversion of the covariance matrix and (as we shall see below) permits their evaluation without the need to truncate the data. There is a need to invert $\mathbf{\Sigma}$ to obtain the inverses $\mathbf{Z}^{-1}$ (which are required to solve the inverse problem), but as one can obtain $\mathbf{W}^{-1}$ as the eigenvectors of $\hat{\mathbf{C}}^{\mathrm{T}}$, this only involves dividing by the singular values, rather than by the square of the singular values, and the procedure is thus less ill-conditioned.

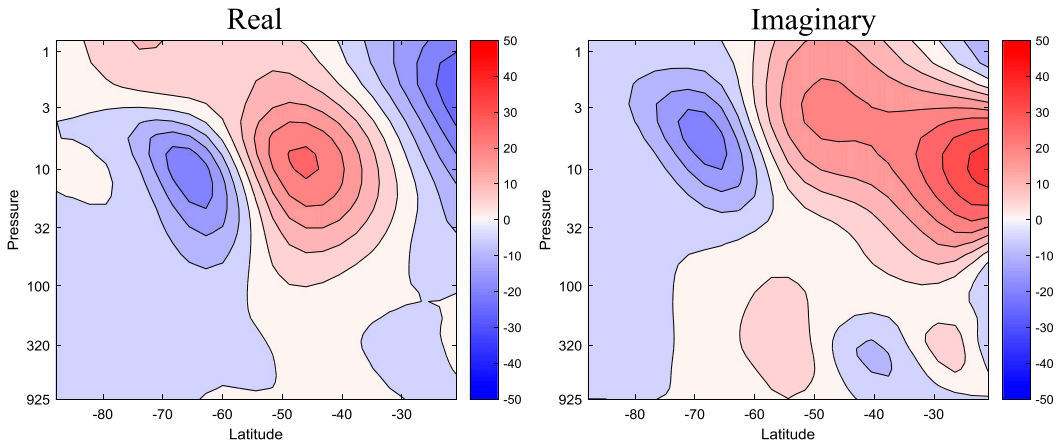

FIG. 4. (left) Real and (right) imaginary parts of the leading stratospheric mode for the unforced case. The eigenvalue associated with this mode corresponds to a decay time of 66 days and a period of propagation of 658 days.

As in Sheshadri and Plumb (2017), we find that the results of this analysis are independent of the choice of lag for a range of lags lying between 20 days and a longer time scale set by when the cross correlations become close to 0. The POP structures are deweighted and the POPs of interest are selected by maximizing the projection of these structures onto those of the leading two EOFs. Tropospheric (stratospheric) POPs are selected

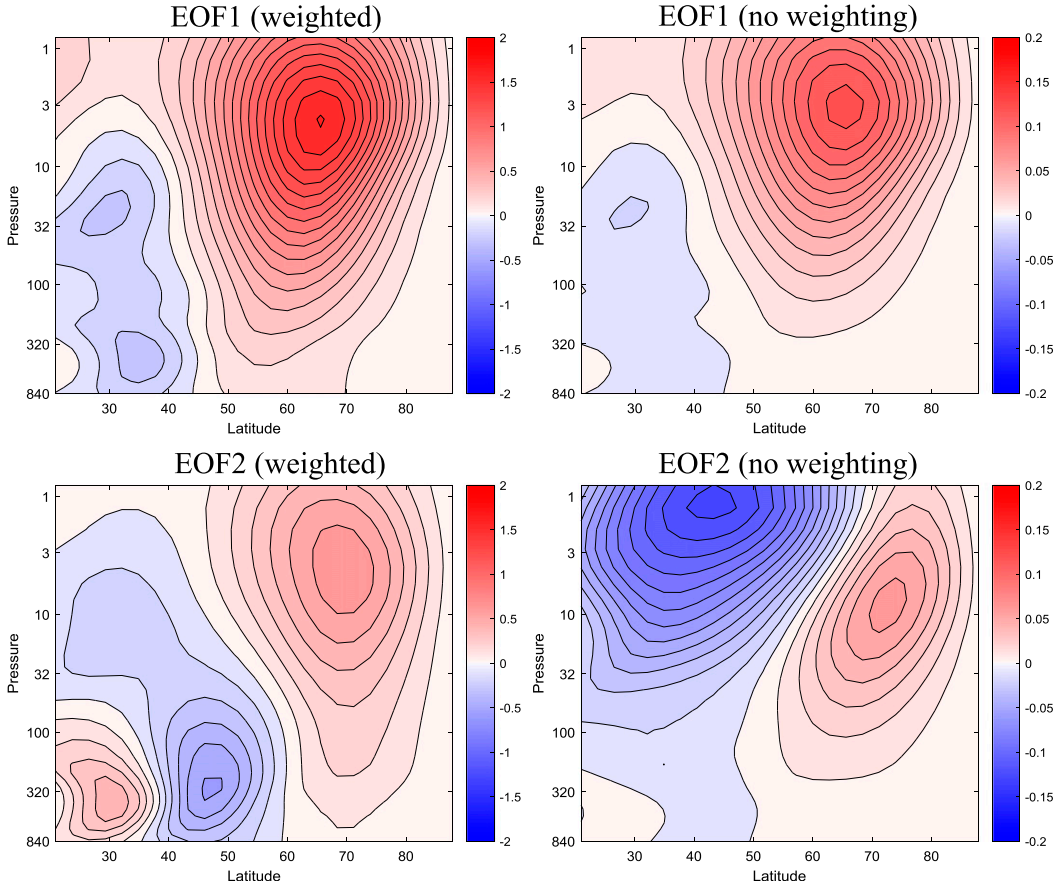

FIG. 5. The two leading EOFs of (left) pressure-weighted zonal-mean zonal wind and (right) zonal-mean zonal wind without any pressure weighting, from the forced integration. The EOFs in the left panels explain (top) 43.5% and (bottom) 17% of variance and have decorrelation times of 80 and 17 days, respectively; while the EOFs in the right panels explain (top) 64% and (bottom) 11.6% of variance and have decorrelation times of 54 and 13 days, respectively.

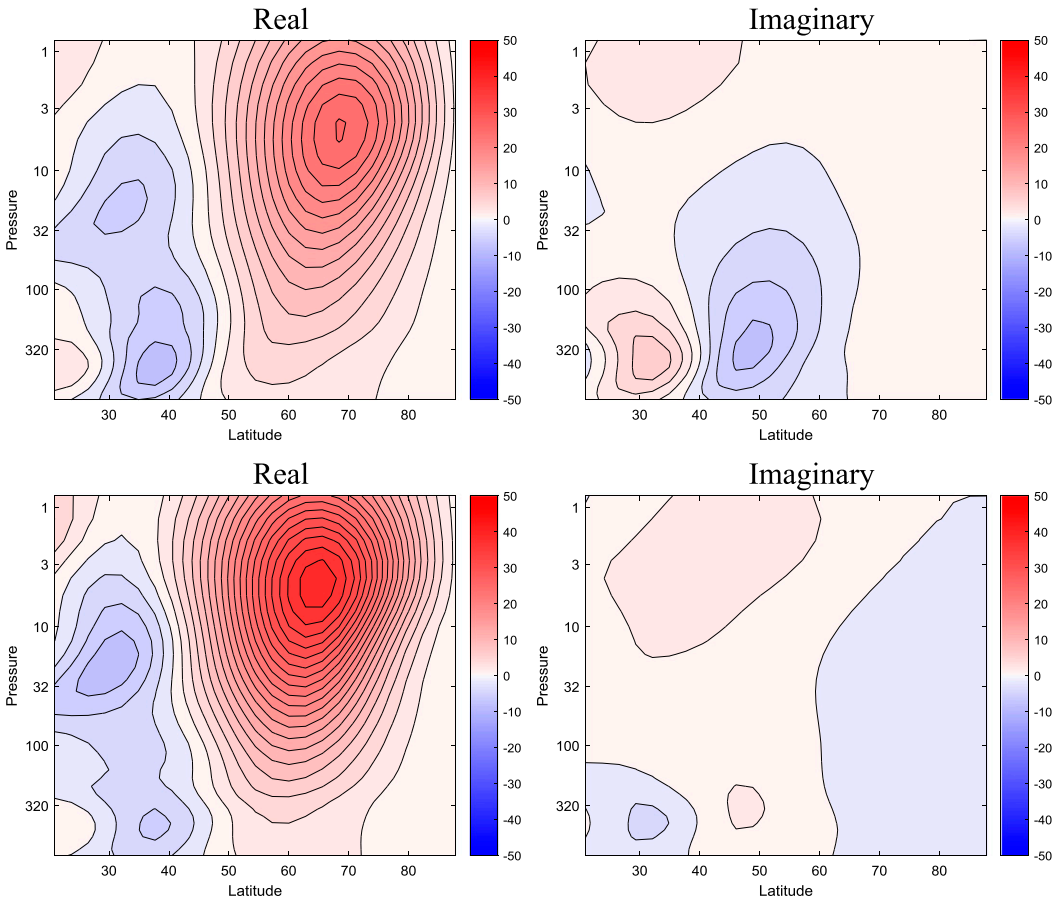

FIG. 6. The structures of the leading (top) tropospheric and (bottom) stratospheric POPs for the forced integration. Their eigenvalues correspond to a decay time scale of 30 days and a period of propagation of 118 days for the tropospheric mode and a decay time of 132 days and a period of propagation of 1160 days for the stratospheric mode.

by maximizing projections onto the first two EOFs of pressure-weighted (non–pressure weighted) zonal wind data using

$$\mathbf{U} = \mathbf{Z}(\mathbf{\Sigma W})^{-1}. \tag{12}$$

Appendix A in Sheshadri and Plumb (2017) shows analytically that the structure of POPs does not change with weighting, a factor that is particularly important for a deep system such as the troposphere and stratosphere. This result is dependent on using all EOFs for the analysis. We now demonstrate this using an example of a mode from the analysis of the unforced integration. Figure 2 shows the structure of the two leading EOFs computed from zonal-mean zonal wind data with and without pressure weighting from this run. It is evident that tropospheric variability is emphasized in the EOF structures computed from pressure-weighted data, and vice versa. The decorrelation time scales associated with these two leading patterns also change quite significantly between these EOFs: 19 and 13 days for the pressure-weighted data but 40 and 17 days without the weighting. In contrast, the POPs calculated from zonal wind data with and without the pressure weighting are identical (Fig. 3 shows the leading tropospheric POP calculated both ways), as are their associated eigenvalues (which imply a time scale of decay of 39 days and a propagation time scale of 126 days). The POP structures (which can be arbitrarily normalized) shown in Fig. 3 are scaled by the value of the respective eigenvectors at the same grid point in all cases.

4. POP structures in space and time

The time evolution of anomaly patterns cannot be captured by a single EOF; however, it is possible to examine the evolution of POP structures in time. In movies S1–S4 in the online supplemental material, we present the oscillatory component of the leading

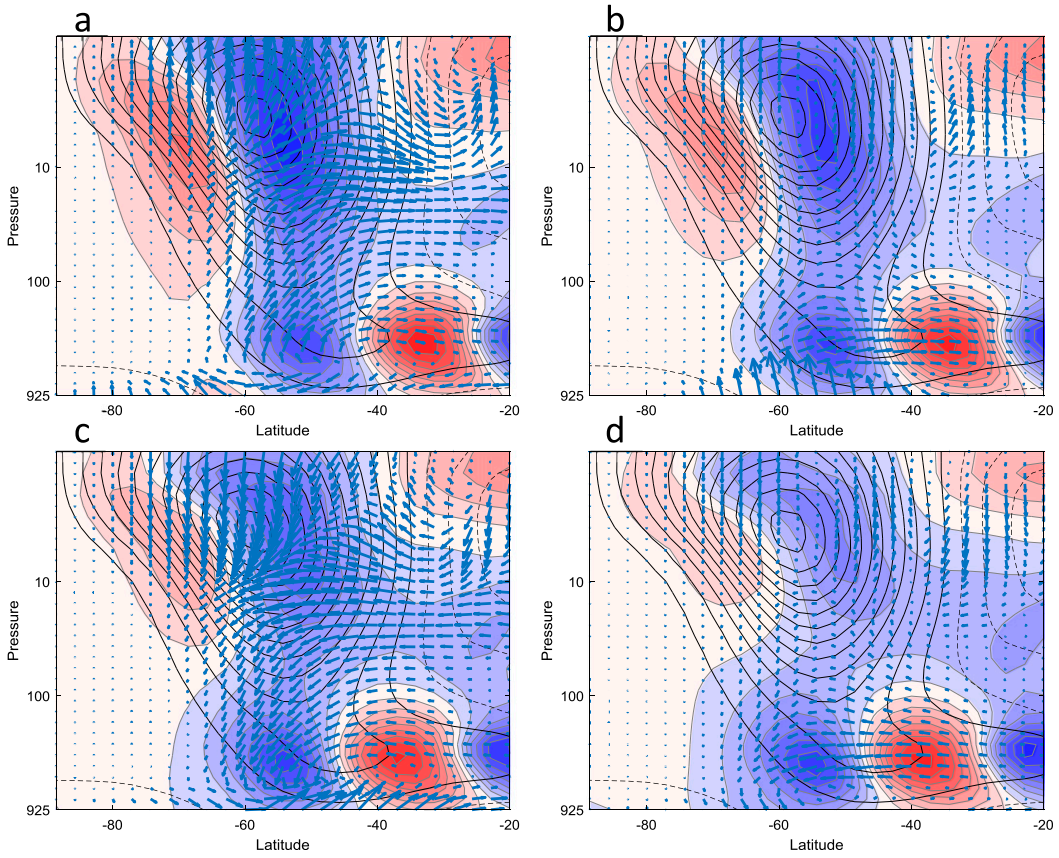

FIG. 7. Snapshots of the oscillatory component of the leading tropospheric mode in the unforced integration at phases of (a) 0, (b) $\pi/2$, (c) π, and (d) $3\pi/2$, with the associated EP flux anomalies superimposed.

tropospheric and stratospheric POPs for both integrations. As in the previous section, the leading tropospheric and stratospheric POPs are chosen by maximizing their projections onto the leading EOFs calculated from pressure-weighted and non-pressure-weighted zonal-mean zonal wind data. Superimposed on these structures is the Eliassen–Palm (EP) flux anomaly associated with the phases of the mode from 0 to 8π, calculated using the coefficients that weight the EOFs to form the POP of interest. Snapshots of these movies at phases of 0, $\pi/2$, π, and $3\pi/2$ are shown later (see Figs. 7–10). If the POPs are expressed in terms of the EOFs as $\mathbf{Z} = \mathbf{UB}$, where $\mathbf{B}$ are the coefficients, then the mode Z_n is

$$Z_n = \mathrm{Re}\,(Z_{in}e^{-i\omega t}) = \mathrm{Re}\,(Z_{in}e^{i\phi}) = \mathrm{Re}\left(\sum_m U_{im}B_{mn}e^{i\phi}\right), \tag{13}$$

where ϕ is the phase. The horizontal and vertical components of the EP flux F^{yz} can be regressed onto the PCs as $F^{yz} = G^{yz}\mathbf{V}^{\mathrm{T}}$, which, when combined with (13), gives the EP flux anomaly associated with the phase ϕ of mode Z_n as

$$F^{Z_n}_{yz} = \sum_m \frac{G^{yz}_{im}}{\sigma_m}\mathrm{Re}\,(B_{mn}e^{i\phi}). \tag{14}$$

In the unforced integration, EOF1 calculated from pressure-weighted zonal-mean zonal wind data shows the familiar dipolar pattern of anomalies straddling the time-mean midlatitude jet in the troposphere, whereas EOF1 calculated from data that have not been pressure weighted is dominated by stratospheric anomalies (Fig. 2). EOF2 in the pressure-weighted case captures the pulsing of the jet in the troposphere and anomalies straddling the jet in the stratosphere, but tropospheric jet shifts and stratospheric jet pulsing in the calculation without pressure weighting. The real and imaginary parts of the leading tropospheric POP for this integration are shown in Fig. 3, and Fig. 4 shows the real and imaginary parts of the leading stratospheric POP.

In the forced integration, EOF1 and EOF2 calculated from pressure-weighted data (shown in Fig. 5) show

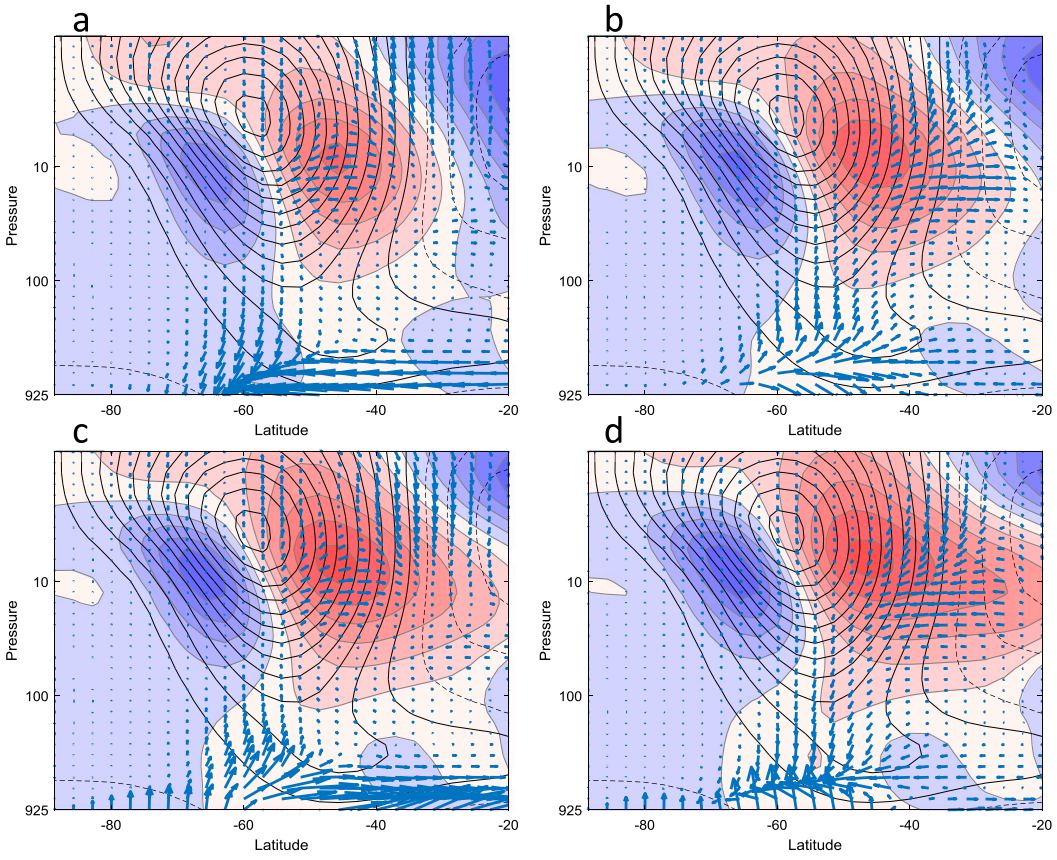

FIG. 8. Snapshots of the oscillatory component of the leading stratospheric mode in the unforced integration at phases of (a) 0, (b) $\pi/2$, (c) π, and (d) $3\pi/2$, with the associated EP flux anomalies superimposed.

pulsing in the stratosphere with tropospheric extensions corresponding to jet shifts and jet pulsing in the troposphere, respectively. The leading two EOFs calculated from zonal wind data that are not pressure weighted are both dominated by stratospheric variability, with EOF1 describing changes in the strength of the stratospheric jet and EOF2 showing anomalies straddling the jet. Movies S3 and S4 show the oscillatory component of the leading tropospheric and stratospheric POPs for the forced integration, with snapshots of the real and imaginary parts of these modes shown in Fig. 6.

Snapshots of the oscillatory components of the leading tropospheric and stratospheric modes in the unforced and forced integrations at phases of 0, $\pi/2$, π, and $3\pi/2$ are also shown (Figs. 7–10). The fast, tropospheric, mode looks much the same in the two cases and describes sustained poleward propagation in the troposphere, and a strong stratospheric response at a certain phase of the tropospheric signal (movies S1 and S3). In the unforced case, the anomaly in zonal-mean zonal wind extends up to the stratosphere when the tropospheric anomaly is in phase with the climatological tropospheric jet. In the forced integration, it occurs when the tropospheric node coincides with the jet. This may be because in the forced case, the stratospheric jet is farther poleward so the tropospheric anomaly has to be farther poleward to trigger a stratospheric response. The EP flux anomalies over the course of the evolution of this mode in the troposphere are broadly consistent with Sparrow et al. (2009) and the propagating regime described by Lee et al. (2007), with EP fluxes transitioning from being anomalously upward to downward in phase with changes in the sign of wind anomalies (movies S1 and S3; Figs. 7, 9). The location of anomalous upward EP fluxes (the EP flux source) migrates with the wind anomalies; this effect is likely to be enhanced at low frequencies (Sparrow et al. 2009; Boljka et al. 2018).

The slower mode seems to be a stratospheric mode with a tropospheric response. It changes in character. In the unforced case, it is a latitudinal shift of the stratospheric jet. While the associated EP flux anomalies do switch from upward to downward in phase with the vortex pulsing, the mode has little tropospheric signal (movie S2; Fig. 8). This behavior is reminiscent of the

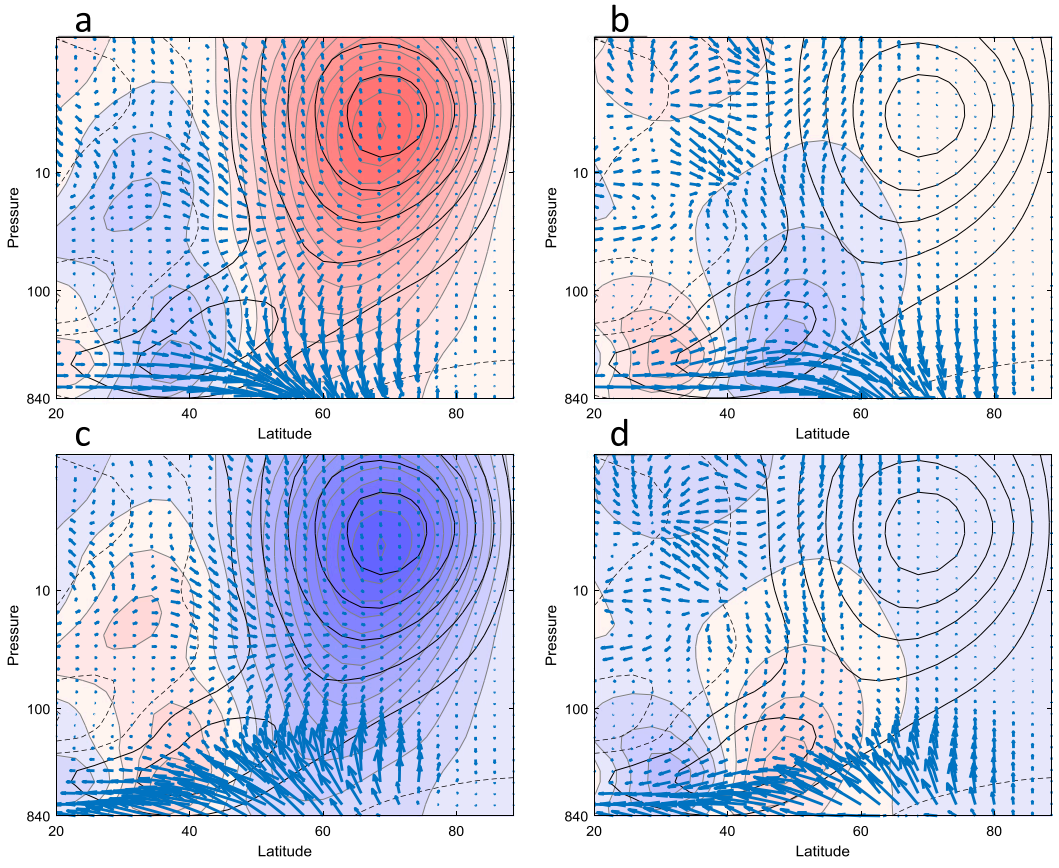

FIG. 9. Snapshots of the oscillatory component of the leading tropospheric mode in the forced integration at phases of (a) 0, (b) $\pi/2$, (c) π, and (d) $3\pi/2$, with the associated EP flux anomalies superimposed.

observed Southern Hemisphere in midwinter, at which time stratosphere–troposphere coupling is not thought to be strong. For the forced case, it is more of a strengthening/weakening in the stratosphere but with a tropospheric extension. It is propagating in the forced case but so slowly that in practice the mode will have decayed away before a length of time corresponding to the period of the mode has passed. The EP flux anomalies associated with this mode bear a qualitative resemblance to those associated with SSW life cycles (e.g., Limpasuvan et al. 2004). Increased upward EP flux anomalies are evident above 100 hPa, indicating a period of increased planetary wave propagation into the stratosphere, followed by anomalously low wave activity as the vortex recovers and the EP flux anomalies transition into being downward (movie S4; Fig. 10). Both anomalously strong and weak vortex events appear to be followed by like-signed anomalies in the mode all the way to the surface. This cycle of wind and EP flux anomalies is reminiscent of the vacillation cycles reported by Kodera et al. (2000), Kodera and Kuroda (2000), and Kuroda (2002). The coincidence of downward migration of zonal flow anomalies with downward EP fluxes (total EP fluxes, not shown) suggests that this vacillation cycle could be stratospherically driven.

5. Discussion and conclusions

The robustness of POPs to pressure weighting of the zonal wind data makes them more meaningful than EOFs while considering the variability of the deep troposphere–stratosphere system. The structure of EOFs, in contrast, changes from being predominantly tropospheric with pressure weighting to stratospheric without weighting. One could compute EOFs level by level (e.g., Baldwin and Dunkerton 2001; Gerber et al. 2010), but their sign is arbitrary and has to be manually adjusted level by level, making it difficult to follow the progression of anomalies in time between the troposphere and stratosphere.

POPs show time structure in addition to structure in latitude and pressure, making it possible to interpret interactions between the troposphere and stratosphere. The analysis in this manuscript has revealed the

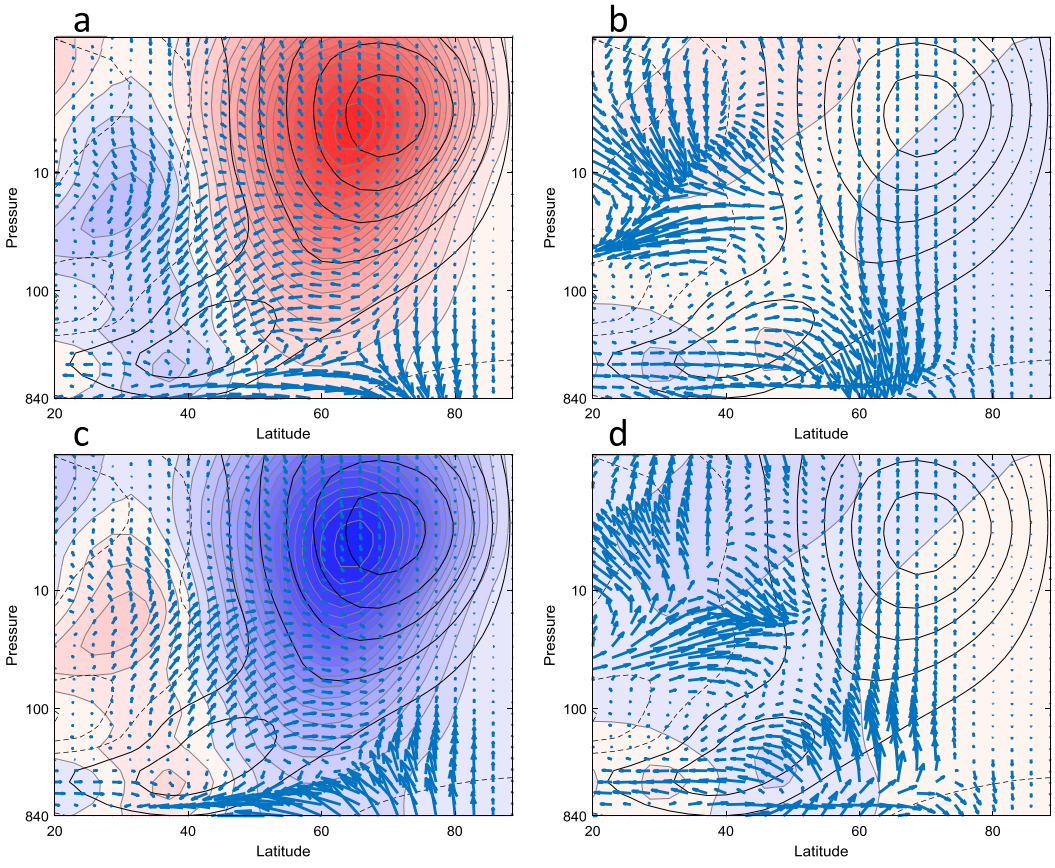

FIG. 10. Snapshots of the oscillatory component of the leading stratospheric mode in the forced integration at phases of (a) 0, (b) $\pi/2$, (c) π, and (d) $3\pi/2$, with the associated EP flux anomalies superimposed.

existence of separate tropospheric and stratospheric modes in integrations that are both Northern Hemisphere like and Southern Hemisphere like. In the unforced case, there seems to be little impact of stratospheric variability on the troposphere in this midwinter situation—resembling the observed Southern Hemisphere in which the troposphere and stratosphere are not thought to be strongly coupled in midwinter. In the strongly forced case, a mode emerges that captures stratospheric vacillation cycles that are associated with similarly signed anomalies in the troposphere. The mode shows that both anomalously weak and anomalously strong vortex events are associated with like-signed anomalies through the depth of the troposphere, all the way to the surface, much like the observed Northern Hemisphere in midwinter.

Acknowledgments. This work was partially supported by Junior Fellow Award 354584 from the Simons Foundation to AS and by the National Science Foundation through Grant OCE-1338814 to MIT. Support from the Swiss National Science Foundation to DD through Grant PP00P2_170523 is gratefully acknowledged. We thank Rachel White for useful discussions; Kunal Mukherjee for assistance with the movies; and three anonymous reviewers for their constructive comments, which greatly improved the manuscript.

REFERENCES

Baldwin, M. P., and T. J. Dunkerton, 1999: Propagation of the Arctic Oscillation from the stratosphere to the troposphere. *J. Geophys. Res.*, **104**, 30 937–30 946, https://doi.org/10.1029/1999JD900445.

——, and ——, 2001: Stratospheric harbingers of anomalous weather regimes. *Science*, **294**, 581–584, https://doi.org/10.1126/science.1063315.

——, D. B. Stephenson, D. W. J. Thompson, T. J. Dunkerton, A. J. Charlton, and A. O'Neill, 2003: Stratospheric memory and skill of extended-range weather forecasts. *Science*, **301**, 636–640, https://doi.org/10.1126/science.1087143.

Boljka, L., T. G. Shepherd, and M. Blackburn, 2018: On the coupling between barotropic and baroclinic modes of extratropical atmospheric variability. *J. Atmos. Sci.*, **75**, 1853–1871, https://doi.org/10.1175/JAS-D-17-0370.1.

Byrne, N. J., T. G. Shepherd, T. Woolings, and R. A. Plumb, 2016: Annular modes and apparent eddy feedbacks in the

Southern Hemisphere. *Geophys. Res. Lett.*, **43**, 3897–3902, https://doi.org/10.1002/2016GL068851.

——, ——, T. Woollings, and R. A. Plumb, 2017: Nonstationarity in Southern Hemisphere climate variability associated with the seasonal breakdown of the stratospheric polar vortex. *J. Climate*, **30**, 7125–7139, https://doi.org/10.1175/JCLI-D-17-0097.1.

Charlton, A., and L. M. Polvani, 2007: A new look at stratospheric sudden warmings. Part I: Climatology and modeling benchmarks. *J. Climate*, **20**, 449–469, https://doi.org/10.1175/JCLI3996.1.

Chen, G., and R. A. Plumb, 2009: Quantifying the eddy feedback and the persistence of the zonal index in an idealized atmospheric model. *J. Atmos. Sci.*, **66**, 3707–3720, https://doi.org/10.1175/2009JAS3165.1.

Gerber, E. P., and Coauthors, 2010: Stratosphere-troposphere coupling and annular mode variability in chemistry-climate models. *J. Geophys. Res.*, **115**, D00M06, https://doi.org/10.1029/2009JD013770.

Gritsun, A., and G. Branstator, 2007: Climate response using a three-dimensional operator based on the fluctuation–dissipation theorem. *J. Atmos. Sci.*, **64**, 2558–2575, https://doi.org/10.1175/JAS3943.1.

Hassanzadeh, P., and Z. Kuang, 2016: The linear response function of an idealized atmosphere. Part II: Implications for the practical use of the fluctuation–dissipation theorem and the role of operator's nonnormality. *J. Atmos. Sci.*, **73**, 3441–3452, https://doi.org/10.1175/JAS-D-16-0099.1.

Held, I. M., and M. J. Suarez, 1994: A proposal for the intercomparison of the dynamical cores of atmospheric general circulation models. *Bull. Amer. Meteor. Soc.*, **75**, 1825–1830, https://doi.org/10.1175/1520-0477(1994)075<1825:APFTIO>2.0.CO;2.

Kodera, K., and Y. Kuroda, 2000: A mechanistic model study of slowly propagating coupled stratosphere-troposphere variability. *J. Geophys. Res.*, **105**, 12 361–12 370, https://doi.org/10.1029/2000JD900094.

——, ——, and S. Pawson, 2000: Stratospheric sudden warmings and slowly propagating zonal-mean zonal wind anomalies. *J. Geophys. Res.*, **105**, 12 351–12 359, https://doi.org/10.1029/2000JD900095.

Kuroda, K., 2002: Relationship between the polar-night oscillation and the annular mode. *Geophys. Res. Lett.*, **29**, 1240, https://doi.org/10.1029/2001GL013933.

Lee, S., S. W. Son, K. Grise, and S. B. Feldstein, 2007: A mechanism for the poleward propagation of zonal mean flow anomalies. *J. Atmos. Sci.*, **64**, 849–868, https://doi.org/10.1175/JAS3861.1.

Limpasuvan, V., D. J. Thompson, and D. L. Hartmann, 2004: The life cycle of the Northern Hemisphere sudden stratospheric warmings. *J. Climate*, **17**, 2584–2596, https://doi.org/10.1175/1520-0442(2004)017<2584:TLCOTN>2.0.CO;2.

Lorenz, D. J., and D. L. Hartmann, 2001: Eddy–zonal flow feedback in the Southern Hemisphere. *J. Atmos. Sci.*, **58**, 3312–3327, https://doi.org/10.1175/1520-0469(2001)058<3312:EZFFIT>2.0.CO;2.

——, and ——, 2003: Eddy–zonal flow feedback in the Northern Hemisphere winter. *J. Climate*, **16**, 1212–1227, https://doi.org/10.1175/1520-0442(2003)16<1212:EFFITN>2.0.CO;2.

Lutsko, N. J., I. M. Held, and P. Zurita-Gotor, 2015: Applying the fluctuation–dissipation theorem to a two-layer model of quasigeostrophic turbulence. *J. Atmos. Sci.*, **72**, 3161–3177, https://doi.org/10.1175/JAS-D-14-0356.1.

Martynov, R. S., and Y. M. Nechepurenko, 2004: Finding the response matrix for a discrete linear stochastic dynamical system. *J. Comput. Math. Phys.*, **44**, 771–781.

Newman, M., and P. D. Sardeshmukh, 2008: Tropical and stratospheric influences on extratropical short-term climate variability. *J. Climate*, **21**, 4326–4347, https://doi.org/10.1175/2008JCLI2118.1.

Penland, C., 1989: Random forcing and forecasting using principal oscillation pattern analysis. *Mon. Wea. Rev.*, **117**, 2165–2185, https://doi.org/10.1175/1520-0493(1989)117<2165:RFAFUP>2.0.CO;2.

——, and P. D. Sardeshmukh, 1995: The optimal growth of tropical sea surface temperature anomalies. *J. Climate*, **8**, 1999–2024, https://doi.org/10.1175/1520-0442(1995)008<1999:TOGOTS>2.0.CO;2.

Polvani, L. M., and P. J. Kushner, 2002: Tropospheric response to stratospheric perturbations in a relatively simple general circulation model. *Geophys. Res. Lett.*, **29**, 1114, https://doi.org/10.1029/2001GL014284.

Ring, M. J., and R. A. Plumb, 2007: Forced annular mode patterns in a simple atmospheric general circulation model. *J. Atmos. Sci.*, **64**, 3611–3626, https://doi.org/10.1175/JAS4031.1.

——, and ——, 2008: The response of a simplified GCM to axisymmetric forcings: Applicability of the fluctuation–dissipation theorem. *J. Atmos. Sci.*, **65**, 3880–3898, https://doi.org/10.1175/2008JAS2773.1.

Scaife, A. A., and I. N. James, 2000: Response of the stratosphere to interannual variability of tropospheric planetary waves. *Quart. J. Roy. Meteor. Soc.*, **126**, 275–297, https://doi.org/10.1002/qj.49712656214.

——, and Coauthors, 2016: Seasonal winter forecasts and the stratosphere. *Atmos. Sci. Lett.*, **17**, 51–56, https://doi.org/10.1002/asl.598.

Scott, R. K., and L. M. Polvani, 2006: Internal variability of the winter stratosphere. Part I: Time-independent forcing. *J. Atmos. Sci.*, **63**, 2758–2776, https://doi.org/10.1175/JAS3797.1.

Sheshadri, A., and R. A. Plumb, 2016: Sensitivity of the surface responses of an idealized AGCM to the timing of imposed ozone depletion-like polar stratospheric cooling. *Geophys. Res. Lett.*, **43**, 2330–2336, https://doi.org/10.1002/2016GL067964.

——, and ——, 2017: Propagating annular modes: Empirical orthogonal functions, principal oscillation patterns, and time scales. *J. Atmos. Sci.*, **74**, 1345–1361, https://doi.org/10.1175/JAS-D-16-0291.1.

——, ——, and E. P. Gerber, 2015: Seasonal variability of the polar stratospheric vortex in an idealized AGCM. *J. Atmos. Sci.*, **72**, 2248–2266, https://doi.org/10.1175/JAS-D-14-0191.1.

Sparrow, S., M. Blackburn, and J. D. Haigh, 2009: Modes of variability in the atmosphere and eddy–zonal flow interactions. Part I: High- and low-frequency behavior. *J. Atmos. Sci.*, **66**, 3075–3094, https://doi.org/10.1175/2009JAS2953.1.

Thompson, D. W. J., and J. M. Wallace, 2000: Annular modes in the extratropical circulation. Part I: Month-to-month variability. *J. Climate*, **13**, 1000–1016, https://doi.org/10.1175/1520-0442(2000)013<1000:AMITEC>2.0.CO;2.

——, ——, and G. C. Hegerl, 2000: Annular modes in the extratropical circulation. Part II: Trends. *J. Climate*, **13**, 1018–1036, https://doi.org/10.1175/1520-0442(2000)013<1018:AMITEC>2.0.CO;2.

Tripathi, O. P., and Coauthors, 2015: The predictability of the extratropical stratosphere on monthly time-scales and its impact on the skill of tropospheric forecasts. *Quart. J. Roy. Meteor. Soc.*, **141**, 987–1003, https://doi.org/10.1002/qj.2432.

von Storch, H., and J. Xu, 1990: Principal oscillation pattern analysis of the tropical 30 to 60 day oscillation in the tropical troposphere. Part I: Definition of an index and its prediction. *Climate Dyn.*, **4**, 175–190, https://doi.org/10.1007/BF00209520.

——, T. Bruns, I. Fischer-Burns, and K. Hasselmann, 1988: Principal oscillation pattern analysis of the 30- to 60-day oscillation in a GCM equatorial troposphere. *J. Geophys. Res.*, **93**, 11 020–11 036, https://doi.org/10.1029/JD093iD09p11022.

Xu, J., and H. von Storch, 1990: Predicting the state of the Southern Oscillation using principal oscillation pattern analysis. *J. Climate*, **3**, 1315–1329, https://doi.org/10.1175/1520-0442(1990)003<1316:PTSOTS>2.0.CO;2.